

Linking reduced breaking crest speeds to unsteady nonlinear water wave group behavior

M.L. Banner^{1*}, X. Barthelemy^{1,2}, F. Fedele³, M. Allis², A. Benetazzo⁴, F. Dias⁵ and W.L. Peirson².

1. School of Mathematics and Statistics, The University of New South Wales, Sydney 2052, Australia

2. Water Research Laboratory, School of Civil and Environmental Engineering, The University of New South Wales, Manly Vale, NSW 2093, Australia

3. School of Civil and Environmental Engineering, and School of Electrical and Computer Engineering, Georgia Institute of Technology, Atlanta, GA 30332, USA.

4. Institute of Marine Sciences, National Research Council (CNR-ISMAR), Venice, Italy.

5. UCD School of Mathematical Sciences, University College Dublin, Belfield, Dublin 4, Ireland.

1 **Abstract**

2 Observations show that maximally-steep breaking water wave crest speeds are much slower than
3 expected. We report a wave-crest slowdown mechanism generic to *unsteady* propagating deep water
4 wave groups. Our fully nonlinear computations show that just prior to reaching its maximum height, each
5 wave crest slows down significantly and either breaks at this reduced speed, or accelerates forward
6 unbroken. This finding is validated in our extensive laboratory and field observations. This behavior
7 appears to be generic to unsteady dispersive wave groups in other natural systems.

8

9 **Introduction**

10 Nonlinear wave groups occur in a wide range of natural systems, exhibiting complex behaviors
11 especially in focal zones where there is rapid wave energy concentration and possible ‘wave-breaking’.
12 The incompletely-understood interplay between dispersion, directionality and nonlinearity presents a
13 significant knowledge gap presently beyond analytical treatment. Here, we investigate maximally-steep,

14 deep-water wave group behaviour, but the findings appear relevant to dispersive nonlinear wave motion
 15 in many other natural systems.

16 In the open ocean, wind forcing generates waves that can steepen and break conspicuously as
 17 whitecaps, strongly affecting fundamental air-sea exchanges, including greenhouse gases. This has
 18 stimulated recent interest in measuring whitecap properties spectrally. While accurately measuring
 19 wavelengths of individual breakers is difficult, measuring whitecap *speeds* can provide a less direct but
 20 more convenient method: since a whitecap remains attached to the underlying wave crest during active
 21 breaking. The dispersion relation from Stokes' classical deep water wave theory discussed below (Stokes
 22 [1]) conventionally provides the wavelength from the observed whitecap speed (Phillips [2]).

23 Stokes' theory was developed for a *steady*, uniform train of two-dimensional (2D) non-linear, deep-
 24 water waves of small-to-intermediate mean steepness ak ($=2\pi\times\text{amplitude}/\text{wavelength}$), for which the
 25 intrinsic wave speed c increases slowly with ak :

$$26 \quad c = c_0[1+1/2 (ak)^2+\text{higher order terms in } (ak)]^{1/2} \quad (1)$$

27 where c_0 is the wave speed for linear (infinitesimally-steep) waves. Extending (1) computationally to
 28 maximally-steep, steady waves (Longuet-Higgins [3]), c approaches $1.1c_0$. Thus, increased wave
 29 steepness has long been associated with *higher* wave speeds.

30 Natural wind-waves comprise a spectrum of modes interacting on different scales, producing evolving
 31 wave-group patterns rather than steady, uniform wavetrains (Longuet-Higgins [4]). Here we investigate
 32 the 'dominant' waves, i.e. those with the largest spectral amplitudes after filtration of higher-wavenumber
 33 components. Within a group, each advancing dominant wave gradually changes its height and shape,
 34 characterized by slow forward and backward leaning of the crests (Tayfun [5]), also transiently becoming
 35 the tallest wave. This tallest wave may break, or else decrease in height while advancing unbroken
 36 towards the front of the group.

37 In this context, previous deep-water breaking wave laboratory studies (Rapp and Melville [6]; Stansell
 38 and McFarlane [7]; Jessup and Phadnis [8]) suggest that breaking-crest speeds are typically $O(20\%)$

39 lower than expected from linear-wave theory, contrary to the expectation from (1) that steeper breaking
40 waves should propagate faster. Understanding this paradoxical crest slowdown behaviour is central to
41 both refining present knowledge on water-wave propagation and dynamics, and optimal implementation
42 of Phillips' spectral framework for breaking waves (Phillips [2]; Kleiss and Melville [9]; Gemmrich et al.
43 [10]).

44 Historically, an appreciable literature has developed on non-breaking, focusing, deep-water, nonlinear
45 wave packets. However, only the studies of Johannessen and Swan ([11], [12]) identified crest slowdown
46 at focus, reporting an $O(10\%)$ crest-speed slowdown relative to its linear-theory prediction. To understand
47 the underlying physics, the present study investigates how very steep unsteady, non-periodic, deep-water
48 wave groups propagate when frequently-assumed theoretical constraints are relaxed, including steady-
49 state, spatially-uniform or slowly-varying, weakly-nonlinear wavetrain behavior. Our goal was to
50 investigate initial breaker speeds, hence it was crucial to track changes, up to the point of breaking
51 initiation, in dominant wave-crest speeds within evolving nonlinear wave groups.

52

53 **Methodology and results**

54 No presently-available analytic theory can predict the evolution of fully-nonlinear, deep-water wave
55 groups. Our primary research strategy utilized simulations from a fully-nonlinear, 3D numerical wave
56 code, validated against results from our innovative laboratory and ocean-wave observations.

57 Our simulations were generated using a numerical wave tank (Grilli et al. [13]). This boundary element
58 code simulates fully-nonlinear potential flow theory and is able to model extreme water waves to the
59 point of overturning. A programmable wave paddle produces a specific 2D or 3D chirped wave-group
60 structure comprising a prescribed number of carrier waves with given initial amplitudes, wavenumbers,
61 frequencies and phases. This shapes the spatial and temporal bandwidths characterizing the group
62 structure and its spectrum. For the simulations, including the 2D example below, the paddle followed the
63 displacement-motion equation (3) described in Song and Banner [14], with $N=5, 7$ and 9 . We also
64 investigated corresponding laterally-converging 3D chirped packet cases with 10- and 25-wavelength

65 focal distances. In this study, breaking occurred predominantly as sequential spilling events with
 66 occasional local plunging. The complementary wave-basin experiments described below also included
 67 comparable bimodal, modulating nonlinear wave packets specified by equation (2) in [14]. The half-
 68 power bandwidths were $O(8)$ times broader than investigated in [9].

69 Figure 1(a) shows the complex growth behavior experienced by all dominant wave crests evolving
 70 within a representative 2D nonlinear, non-breaking wave group. The initial steepest wave decays and is
 71 replaced by the following growing wave, which grows modestly, then slows down and is replaced by the
 72 annotated faster-growing crest, which evolves to its maximum height and decays. As each new crest
 73 develops, it grows (A-B-C) then slows down and attenuates (C-D), then accelerates (D-E) back to its
 74 original speed while advancing towards the front of the group.

75 Figure 1(b) shows the spatial wave profile in greater detail at the evolution times A-E in Figure 1(a).
 76 The dominant wave grows asymmetrically, initially leaning forward as it steepens within the group. In the
 77 absence of breaking, the steepest wave advances leaning forward, relaxing back to symmetry near its
 78 maximum height (the focal point), then leans backwards past the maximum elevation. Forward-leaning
 79 crests are accompanied by backward leaning troughs, and vice-versa. This leaning is a *generic* feature of
 80 each crest in natural, unsteadily-evolving dispersive nonlinear water wave groups (Tayfun [5]).

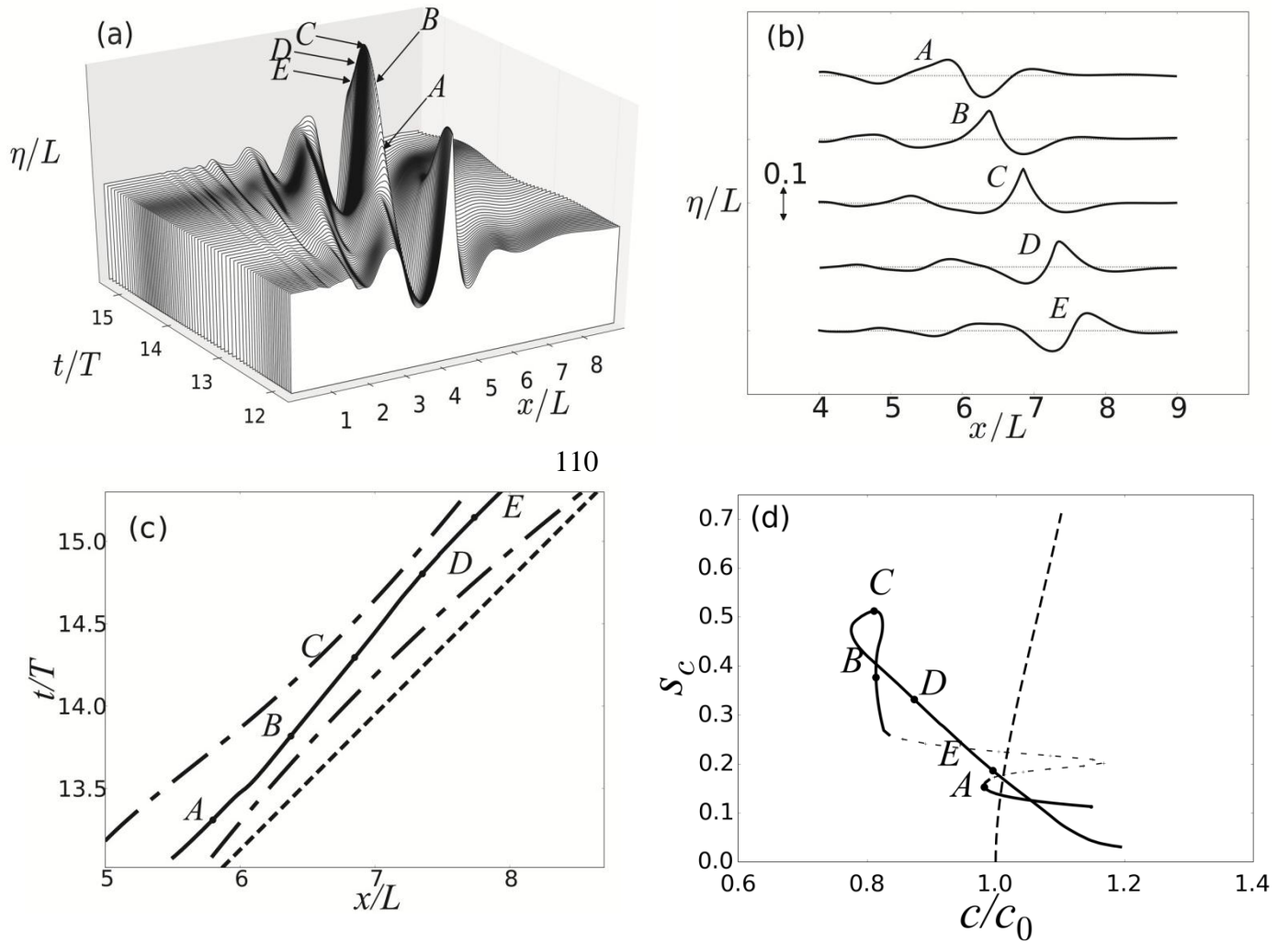
81 Relative to the speed of a classical (symmetrical) Stokes wave, significant crest (and trough) speed
 82 changes accompany the leaning, measured by tracking the (horizontal) speed of a given wave-crest profile
 83 in space and time. The generic crest-speed slowdown is identified in Figure 1(c) by the steeper slope of
 84 the displacement-time curve between B and D relative to the indicated *linear* wave trajectory (speed c_0),
 85 where c_0 is the speed of the spectral peak determined from the computed wave-packet dispersion relation.
 86 The actual speed reduction relative to c_0 is 18%. This lasts about one wave period, with a spatial extent of
 87 about one wavelength. Figure 1(d) shows a typical trajectory when crest speed is plotted against local
 88 crest steepness $s_c = a_c k_c$, where a_c is the time-dependent crest height above mean-water level and the
 89 corresponding local wavenumber k_c is defined as π divided by the local zero-crossing separation spanning

90 the given crest. Introducing s_c was necessary to describe the complexity of *unsteady* nonlinear wave crest
 91 behaviour, and was easily computed for Stokes waves for the crest-speed comparison shown.

92 The significant departure of the crest speed versus crest steepness trajectory for waves in unsteady
 93 wave groups compared with the classical Stokes for steady wavetrain prediction underpins the central
 94 findings in this study. In this example, the maximum crest steepness marginally precedes the slowest
 95 crest speed, with the trajectory looping counter-clockwise about this point. This trajectory is not generic,
 96 since other simulated cases and the experimental curve of Figure 2(b) below showed clockwise looping.
 97 Further studies are needed to explain this effect. Also, as seen in Figure 1(d), the asymmetry of the
 98 dominant wave shape near its maximum steepness results in different crest speeds for growing and
 99 decaying crests of the same steepness. Note that the local peak in crest speed between A and B at $s_c \approx 0.2$ is
 100 an artefact of our crest-tracking algorithm, resulting from the complex crest transition seen in Figure 1(a)
 101 at $(x/L \sim 4, t/T \sim 13.5)$ when the detected crest location jumps abruptly from the receding crest to the newly-
 102 developing crest.

103 The above discussion was for 2D waves, but laterally-focused (3D) wave fronts in both our simulations
 104 and wave-basin investigation (described below) show similar leaning and crest-slowdown behavior, with
 105 the subsequent breaker-crest speed initiated at $\sim 0.8c_0$.

106 Relative to classical ocean-wave speeds, our model results for the speeds of the left-hand and right-
 107 hand zero-crossings spanning the tallest wave shows that their average remains close to the linear wave
 108 speed c_0 (Fig. 1(c)), with modest local fluctuations of (+7% to -1%). Hence, aside from the strong
 109 unsteady leaning crest and trough motions, the waves propagate largely as expected from Stokes theory.



111

112 Figure 1. (a) space-time evolution diagram of a non-breaking 2D chirped wave group, moving toward the
 113 right, showing the decay of the initial tallest crest, growth of the following tallest crest and complex
 114 transitions of other developing crests. Wave properties at annotated times A-E are shown in panels (b), (c)
 115 and (d). T and L are reference carrier-wave period and wavelength scales. (b) tallest crest shapes at
 116 evolution times A-E, showing crest transition from forward-leaning through symmetry to backward-
 117 leaning (c) horizontal location of the tallest crest (solid line) versus time. The steeper slope between B
 118 and D shows the crest-speed reduction relative to c_0 (dotted line). Horizontal locations versus time of the
 119 two adjacent zero-crossings (long-short dashed lines) are also shown. (d) trajectory of the corresponding
 120 tallest crest speed c , normalized by c_0 , against local crest steepness s_c defined in the text. Stokes theory
 121 prediction (1) is shown in terms of s_c (dashed line) for comparison. The apparent crest-speed surge at
 122 $s_c \approx 0.2$ is spurious, as explained in the text.

123

124 *Breaking onset and speed*

125 If the tallest wave in the group proceeds to break rather than recur, our simulations found that breaking
 126 onset occurs when this wave attains maximum steepness and close to its minimum crest speed. This can
 127 certainly explain why initial breaking wave crest speeds are observed to be $O(80\%)$ of the linear carrier-
 128 wave speed (Rapp and Melville [6]; Stansell and McFarlane [7]; Jessup and Phadnis [8]). This behavior
 129 was found in all our simulations and verified in our laboratory measurements (see Figure 2(b)).

130

131 *Is the crest slowdown a nonlinear effect?*

132 Insight on this key question is available from previous linear and weakly-nonlinear theory. For
 133 uniform, deep-water, linear gravity wavetrains, the carrier wave speed c_0 follows from the dispersion
 134 relation $\omega = (gk)^{1/2}$ and $c_0 = \omega_0/k$. However, narrow-band wave groups are characterized by non-
 135 uniformity in both space and time. Correct to $O(v^2)$, a local frequency can be defined (Chu and Mei [15])
 136 as

$$137 \quad \omega = (gk)^{1/2} - \beta a_{xx}/(ak) \quad (2)$$

138 where v is a characteristic spectral bandwidth, $\beta = dc_g/dk$, $c_g = d\omega_0/dk$ is the linear group velocity and $a(x,t)$
 139 is the wavetrain envelope that satisfies the linear Schrödinger equation (Mei [16]). The associated local
 140 phase speed is given approximately by

$$141 \quad c \approx c_0 - \beta a_{xx}/(ak^2). \quad (3)$$

142 Equations (2), (3) and the associated relationships above show that c varies along the group and in time.
 143 Since $\beta < 0$, c attains its lowest value at the envelope maximum, where the largest crest occurs ($a_{xx} < 0$).
 144 The other crests and troughs in the group also experience similar local speed variations.

145 Furthermore, for dispersive, weakly-nonlinear unsteady wave groups, we find that the slowdown effect
146 due to dispersion is counterbalanced by the increase in phase speed due to nonlinearity [Equation (1)],
147 limiting the phase-velocity slowdown within the group (Fedele [17]).

148 Our focus on breaking-crest slowdown for large wave steepness approaching breaking onset is beyond
149 conventional analysis methodologies. We now validate our fully-nonlinear numerical simulation findings
150 on wave-crest slowdown against laboratory and open-ocean measurements.

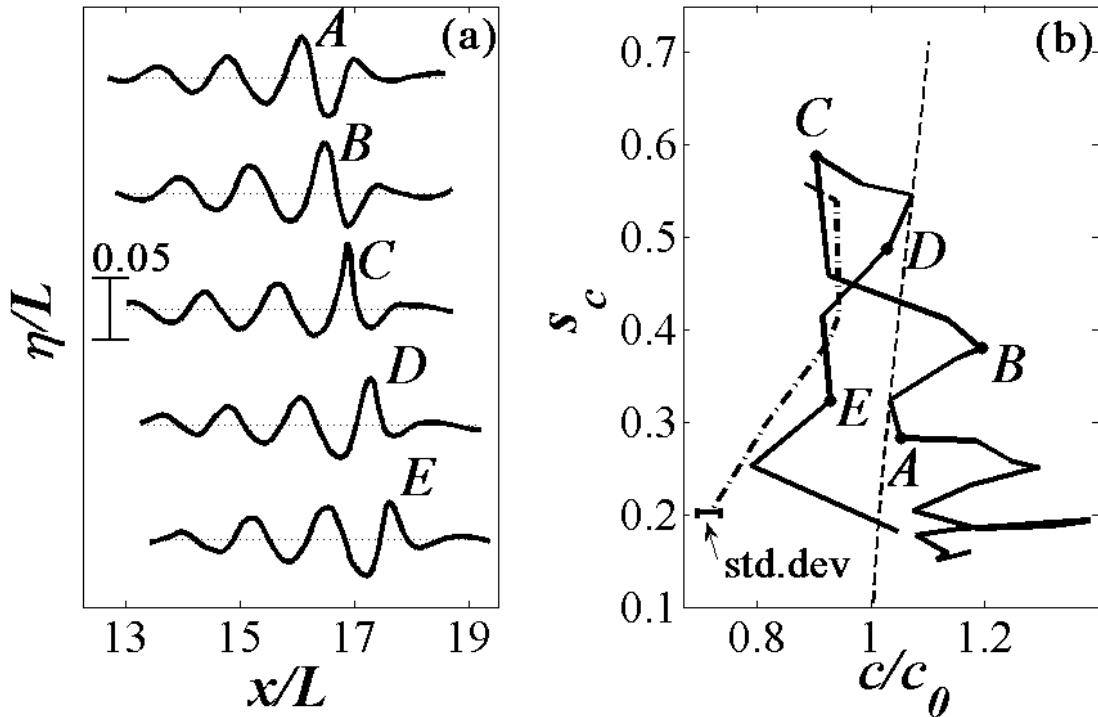
152 *Wave basin measurements*

153 Complementary experiments were performed in a 27m x 7.75m wave basin with 0.55m water depth.
154 Wave groups were generated at one end of the basin by a computer-controlled wave-generator comprising
155 13 bottom-cantilevered, flexible-plate segments. Lateral focusing was achieved by suitably setting the
156 phase of each segment (Dalrymple [18]). A 95% absorbing beach minimized end reflections. Heights of
157 evolving wave groups matching the simulations were measured to within ± 0.5 mm by a traversable in-line
158 array of nine wave-wire probes spanning one wavelength. c_0 was calculated using linear theory from the
159 spectrally-weighted wave frequency of the wave probe closest to the wave-generator.

160 Identified wave crests were tracked between the wave probe signals, their motion interpolated using
161 cubic splining and their crest speeds extracted. An overhead one-megapixel videocamera imaged the
162 breaking crests at 100 Hz. The imagery, corrected for lens and mounting distortion, was transformed onto
163 a regular grid, sequential leading-edge location and lateral extent data were extracted for each breaker and
164 their speeds determined.

165 Figure 2(a) shows surface profiles measured at evolution times A-E, with breaking initiation near C, for
166 a modulating 5-wave, bi-modal breaking case. Figure 2(b) shows its crest speed trajectory. Also shown is
167 the ensemble-mean trajectory for spilling-breaker speeds in the measured ensemble of 240 modulational
168 and chirped 2D and 3D cases. The measurement resolution enabled resolving the crest leaning and
169 slowing at the maximum surface elevation (C). Crest-speed oscillations observed for smaller-steepness
170 waves (e.g. at B), are the same crest-leanings, but occurring earlier as the crest moves through the wave

171 group. This figure confirms the reduced speeds of crests preceding breaking onset and the accompanying
 172 generic breaker slowdown.

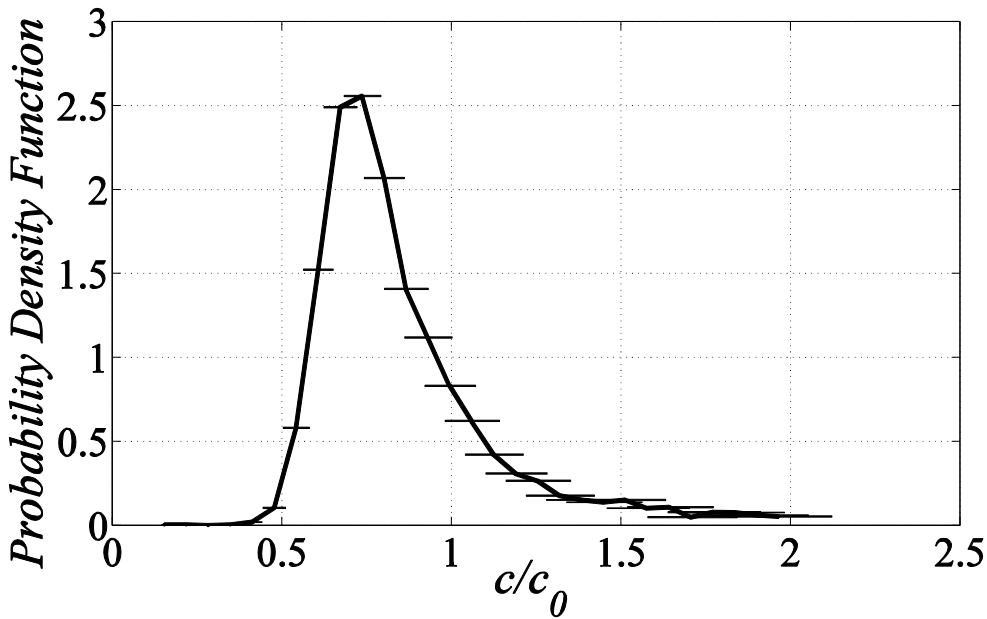


182 Figure 2. (a) measured surface profiles of a 5-wave, bi-modal wave packet, at times A-E, with breaking
 183 initiation at C. (b) corresponding trajectory of normalized crest speed c/c_0 of the tallest wave, against local
 184 crest steepness s_c . The ensemble-mean breaker speed trajectory is shown by the dot-dash line. The dashed
 185 line shows Stokes' prediction. Reference wave scales were $L=1.09\text{m}$, $T=0.836\text{ sec}$.

187 *Open ocean observations*

188 Our *Wave Acquisition Stereo System* (WASS) was deployed at the *Acqua Alta* oceanographic tower 16
 189 km offshore from Venice in 17m water depth (Fedele et al. [19]; Benetazzo et al. [20]). WASS cameras
 190 were 2.5m apart, 12.5m above sea level at 70° depression angle, providing a trapezoidal field-of-view
 191 with sides increasing from 30m to 100m over a 100m fetch. The mean windspeed was 9.6 ms^{-1} with a 110
 192 km fetch. The uni-modal wave spectrum had a significant wave height $H_s=1.09\text{m}$ and dominant period
 193 $T_p=4.59\text{s}$. Most observed crests were very steep, with sporadic spilling breaking. We describe results
 194 using 21,000 frames captured at 10 Hz.

195 The speeds c of crests reaching maximum local steepness within the imaged area were estimated using
 196 a crest-tracking methodology, as in the wave-basin measurements. The data were filtered above 1.5 Hz to
 197 remove short riding waves. Sub-pixeling reduced quantization errors in estimating the local 3D crest
 198 position from the surface-displacement time series spaced along the wave-propagation direction. The
 199 local reference c_0 was calculated from the peak frequency of the short-term Fourier spectrum of a time
 200 series of duration D centered at the crest event, using $D=120\text{sec}$ as a suitable record length and Doppler-
 201 corrected for the in-line 0.20 ms^{-1} mean current. We analyzed 200 dominant local wave crests with
 202 elevations $\eta > 0.3H_s$ and local crest steepness $s_c > 0.3(s_c)_{\max}$ using the observed $(s_c)_{\max}=0.45$, and determined
 203 $\sim 12,000$ evolving crest speeds from a 60-point spatial grid, with 0.5m spacing along the wave-
 204 propagation direction.



214 Figure 3. Probability density function of normalized crest speed c/c_0 for all crests transitioning through a
 215 maximum local crest steepness, from a 35-minute WASS stereo-video sequence from an ocean tower.

216 Note the tall peak at $c/c_0 \sim 0.75$. Local standard error bounds are indicated.

218 Values of D and η were chosen so that the empirical probability density function (pdf) of c/c_0 was
219 insensitive to changes in these parameters. Figure 3 shows the pdf, which peaks at close to $0.75c_0$. Values
220 for $c/c_0 > 1.5$ (7% of the total ensemble) are outliers with $>15\%$ uncertainty in estimating c_0 and crest
221 location. This figure highlights the observed crest slowdown, consistent with the nonlinear simulations
222 and experiments described above.

224 Discussion and conclusions

225 Our study provides fundamental new insights into the behavior of chirped, bi-modal and open-ocean
226 unsteady steep, deep-water nonlinear wave groups. We found that as carrier waves reach maximum
227 steepness, their crests decelerate strongly ($O(20\%)$), which results from unsteady crest sloshing modes
228 arising from the complex interplay between nonlinearity and dispersion. This behaviour departs markedly
229 from the speed increase with wave steepness predicted by steady-wavetrain theory.

230 Our findings have significant, broader consequences. For ocean waves, they explain the puzzling
231 ($O(20\%)$) reduced initial speed of breaking-wave crests, central to assimilating whitecap data accurately
232 into sea-state forecast models. Parameterizations of air-sea fluxes of momentum and energy, which
233 depend on the square and cube of the sea-surface velocity, may be modified appreciably. Atmospheric
234 and oceanic internal waves, (Helfrich and Melville [21]), should also experience similar effects to those
235 described here. As noted above, even weakly-nonlinear, unsteady dispersive water-wave groups described
236 by the nonlinear Schrödinger equation (NLSE) (Zakharov [22]) exhibit crest slowdown. The NLSE is
237 commonly used to describe wave phenomena in other natural systems (e.g. geophysical flows (Osborne
238 [23]), nonlinear optics (Kibler et al. [24], amongst others). Exploring implications of the present findings
239 should provide refined insights when the wave-group nonlinearity and bandwidth are beyond the validity
240 of the NLSE.

243 **References**

- 244 1. Stokes, G.G., 1847. *Trans. Cambridge Phil. Soc.* 8, 441–455.
- 245 2. Phillips, O.M., 1985. *J. Fluid Mech.*, 156, 505–531.
- 246 3. Longuet-Higgins, M.S., 1975. *Proc. Roy. Soc. A* 342, 157–174
- 247 4. Longuet-Higgins, M.S., 1984. *Phil. Trans. R. Soc. A* 310, 219–250.
- 248 5. Tayfun, M, 1986. *J. Geophys. Res.* 91 C6:7743–7752.
- 249 6. Rapp, R.J. and Melville, W.K., 1990. *Phil. Trans. R. Soc. A* 331, 735–800.
- 250 7. Stansell, P. and MacFarlane, C., 2002. *J. Phys. Oceanogr.* 32, 1269–1283.
- 251 8. Jessup, A.T. and Phadnis, K.R., 2005. *Meas. Sci. Technol.* 16, 1961–1969.
- 252 9. Kleiss, J.M. and Melville, W.K., 2010. *J. Phys. Oceanogr.* 40, 2575–2604
- 253 10. Gemmrich, J.R., Zappa, C.J., Banner, M.L. and Morison, R.P. 2013. *J. Geophys. Res. Oceans*,
- 254 In press, doi: 10.1002/jgrc.20334
- 255 11. Johannessen, T.B. and Swan, C., 2001. *Proc. Roy. Soc. Lond. A*, 457, 971–1006.
- 256 12. Johannessen, T.B. and Swan, C., 2003. *Proc. R. Soc. Lond. A*, 459, 1021–1052
- 257 13. Grilli, S., Guyenne, P. and Dias, F., 2001. *Int. J. Num. Methods Fluids*, 35, 829–867.
- 258 14. Song, J. and Banner, M.L., 2002. *J. Phys. Oceanogr.* 32, 2541–2558
- 259 15. Chu, V.H. and Mei, C.C., 1970. *J. Fluid Mech.*, 41, 873–887
- 260 16. Mei, C.C., 1983. *The Applied Dynamics of Ocean Surface Waves*. Wiley-Interscience, 740pp.
- 261 17. Fedele, F., 2013. <http://arxiv.org/abs/1309.0668>
- 262 18. Dalrymple, R.A., 1989. *J. Hydraulic Res.* 27, 23–34.
- 263 19. Fedele, F., Benetazzo, A., Gallego, G., Shih, P.-C., Yezzi, A., Barbariol and F., Arduin, F., 2013. In
- 264 press, <http://dx.doi.org/10.1016/j.ocemod.2013.01.001>
- 265 20. Benetazzo, A., Fedele, F., Gallego, G., Shih, P.C. and Yezzi, A., 2012. *Coastal Engineering*, 64, 127–
- 266 138.
- 267 21. Helfrich, K.R. and Melville, W.K., 2006. *Annu. Rev. Fluid Mech.* 38:395–425.
- 268 22. Zakharov, V. E., 1968. *J. Appl. Mech. Tech. Phys.* 9, 190–194

269 23. Osborne, A.R., 2010. *Nonlinear Ocean Waves and the Inverse Scattering Transform*. Academic Press,
270 ISBN: 978-0-12-528629-9, 949pp.

271 24. Kibler, B., Fatome, J., Finot, C., Millot, G., Genty, G., Wetzel B., Akhmediev, N., Dias F. and
272 Dudley, J.M., 2012. *Nature Scientific Reports* 2:463, DOI: 10.1038/srep00463.

274 **Acknowledgements**

275 Financial support is gratefully acknowledged for XB, MA, MB and WP from the Australian Research
276 Council through their support of Discovery Projects DP0985602, DP120101701. Financial support for
277 MB is also gratefully acknowledged from the National Ocean Partnership Program, through the U.S.
278 Office of Naval Research (Grant N00014-10-1-0390). The WASS experiment at *Acqua Alta* was
279 supported by Chevron (CASE-EJIP Joint Industry Project #4545093). FD was partially supported by ERC
280 under the research project ERC-2011-AdG 290562-MULTIWAVE and SFI under the programme ERC
281 Starter Grant - Top Up, Grant 12/ERC/E2227.

282 In this paper, XB identified and quantified the crest slowdown effect in his steep nonlinear wave
283 computations. MB made the central association with breaker slowdown and was the architect of this
284 paper, coordinating the scientific effort. FF identified that the crest slowdown also occurs in linear wave
285 groups. He revealed that wave group bandwidth and unsteadiness were crucial aspects of the crest
286 slowdown, using linear/nonlinear narrow-band wave theory. MA performed the suite of laboratory wave
287 basin experiments relating crest velocity and breaker speed. AB deployed the WASS, processed stereo
288 data and contributed jointly with FF the WASS ocean wave crest speed analysis. WP and FD made
289 ongoing incisive intellectual contributions.